

# Electrical control of photon spin angular momentum in organic electroluminescent materials

Received: 13 January 2025

Accepted: 19 September 2025

Published online: 26 November 2025

 Check for updates

Francesco Furlan <sup>1,2</sup>, Michal Šámal <sup>3</sup>, Jiří Rybáček <sup>3</sup>, Andrea Taddeucci <sup>4</sup>,  
Marta Di Girolamo <sup>5</sup>, Davide Nodari <sup>1</sup>, Giuliano Siligardi <sup>6</sup>,  
Jessica Wade <sup>2,5</sup>, Binghai Yan <sup>7,8</sup>, Irena G. Stará <sup>3</sup>, Nicola Gasparini <sup>1,2</sup> &  
Matthew J. Fuchter <sup>1,2,9</sup> ✉

The photon spin information encoded in circularly polarized (CP) light is of high interest for current and future technologies, including low-power displays, encrypted communications and high-performance quantum applications. Engineering organic light-emitting diodes (LED) to emit oppositely handed electroluminescent CP light typically requires access to left- and right-handed chiral molecules. In conjugated polymer LEDs, the handedness of CP electroluminescence also depends on the active-layer thickness or direction of current flow. For a given active-layer thickness, it remains unknown whether a single-handed chiral material can emit CP light with opposite handedness in the same LED architecture. Here we demonstrate organic LEDs in which the handedness of the emitted CP electroluminescence can be controlled electrically, solely by using specific interlayers with no change in the emissive material composition or thickness. We reveal that this occurs due to a change in mechanism for the generation of CP electroluminescence, as a function of the recombination zone position within the device. This result provides a paradigm shift in the realization of organic CP-LEDs with controllable spin angular momentum information and further contributes to ongoing discussions relating the fundamental physics of chiral optoelectronics.

Chirality is the property of an object with broken inversion and mirror symmetry, resulting in a pair of non-superimposable mirror image forms. In chemistry, each non-superimposable mirror image of a chiral molecule is called an enantiomer<sup>1</sup>. Chiral materials can absorb, emit and refract circularly polarized light (CPL), which is light with a defined spin angular momentum (SAM). SAM is the intrinsic angular momentum associated to a polarized photon, with a quantized value of  $\pm\hbar$  per photon, corresponding to left- or right-handed circular polarization. Chiral organic semiconductors have recently attracted much interest as the emissive layer in circularly polarized light-emitting diodes (CP-LEDs)<sup>2,3</sup>. Partly due to the encoded SAM, CP-LEDs will

enable multiple technological advances, from the generation of more energy-efficient display technologies to highly precise sensors to devices for quantum information processing and holography<sup>4,5</sup>.

When dealing with thin films of organic emissive chiral materials, the emitted CPL typically occurs through either the intrinsic chiroptical behaviour of the material<sup>1,6,7</sup>—the so-called natural optical activity<sup>8</sup>—or from the selective reflection or birefringence of CPL<sup>9</sup> due to the structural chirality of the film<sup>10–12</sup>. Regardless of which of these mechanisms is operative, the handedness of the emitted CPL from organic chiral materials correlates to the handedness of the enantiomer of the emissive layer: one enantiomeric emitter gives a

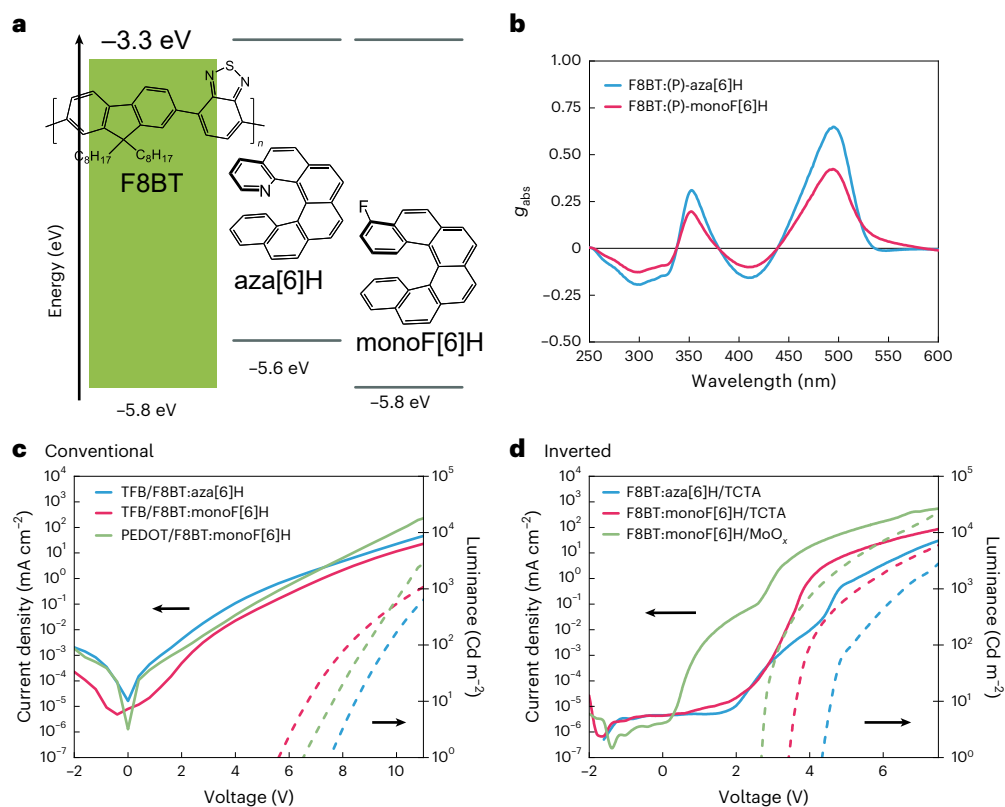


**Fig. 1 | Structure, chiroptical and optoelectronic properties of chiral polymer blends.** **a**, Structure and energy levels of polymer system (F8BT) and chiral additives (aza[6]H or monoF[6]H). **b**, Dissymmetry factor of F8BT:(*P*)-aza[6]H and F8BT:(*P*)-monoF[6]H thin films (160 nm), annealed at 140 °C. **c**, *J*-*V*-*L* characteristics of conventional CP-OLEDs based on F8BT:(*P*)-aza[6]H/(*P*)-monoF[6]H,

with or without TFB as the HTL. **d**, *J*-*V*-*L* characteristics of inverted CP-OLEDs based on F8BT:(*P*)-aza[6]H/(*P*)-monoF[6]H, with or without TCTA as the HTL. Voltage-current density curves are shown as solid lines, and voltage-luminance curves are shown as dashed lines.

CPL of one preferred handedness, whereas the other enantiomer gives equal-magnitude CPL of the opposite handedness<sup>13</sup>. When referring to the emission from a CP-LED, we term this as normal circularly polarized electroluminescence (NCPE).

One of the most successful approaches to realize high circularly polarized electroluminescence (CP-EL) in CP organic light-emitting diodes (OLEDs) has been the use of polymeric thin-film blend materials, where an achiral conjugated polymer is blended with a chiral small-molecule additive<sup>14,15</sup>. We have found the helical small-molecule (*P*)-aza[6]helicene (aza[6]H; Fig. 1a) to be a particularly useful additive to produce films with very high chiroptical activity<sup>16</sup>. While optimizing aza[6]H:polymer blends to improve CP-OLED device efficiencies<sup>16,17</sup>, we discovered a distinct CP-EL mechanism, where the handedness of the CPL emitted inverts as a function of the device architecture (conventional versus inverted) or the emission direction (front or back of the device). This anomalous CP-EL (ACPE)<sup>18</sup> was found to correlate to the directionality of current flow in the device, and was assigned to induced orbital angular momentum (OAM) in the charge carriers, with subsequent transfer to the SAM of the emitted photons. Importantly, ACPE apparently overrode the NCPE of the chiral emissive material. Further details on these mechanisms are provided in Supplementary Note 1.

The interplay between NCPE and ACPE in chiral polymer LEDs remains unclear. From a practical standpoint, exploiting NCPE requires the use of both enantiomers in separate devices to access opposite-handed CPL. Conversely, ACPE requires the use of two different device architectures. It would be a notable advance to be able to access both handedness of CPL from the same enantiomer material in the same device architecture. Here we realize such a goal, demonstrating how CPL handedness can be electrically controlled in a chiral polymer-based CP-OLED. Switching between NCPE and ACPE

is achieved by controlling the charge injection and charge balance through the use of interlayers, and is enabled by a newly developed chiral additive, a monofluorinated [6]helicene ((*P*)-monoF[6]helicene (monoF[6]H); Fig. 1a). NCPE occurs with balanced charge transport in the emissive layer when the recombination zone (RZ) is located in the centre of the device and is independent of the device architecture (that is, conventional or inverted). ACPE occurs with unbalanced charge transport in the emissive layer when the RZ is located close to one of the transport layers (Fig. 1c). To the best of our knowledge, such electrical control of CP-EL has only previously been observed in inorganic materials<sup>19</sup> and in different device configurations (namely, light-emitting transistors). As such, we believe the learnings in this work will enable wholly new directions and progress of CP-OLED device technologies with controllable SAM and contributing to the ongoing studies of chirality-dependent optoelectronic physics<sup>20</sup>.

## Results

Although aza[6]H has proved to be a useful additive to generate blend polymer films with large chiroptical activity, the optoelectronic performance of poly(9,9-dioctylfluorene-*alt*-benzothiadiazole) (F8BT):aza[6]H materials are hindered by the shallower highest occupied molecular orbital of aza[6]H (5.4 eV) compared with the highest occupied molecular orbital of F8BT (5.8 eV; Supplementary Fig. 10 and Supplementary Table 1). This results in aza[6]H acting as a hole trap in the blend, which decreases the device performance and limits the type of device configurations that can be used for working OLEDs. To address this issue, we developed fluorine-substituted monoF[6]H, a chiral additive with a deeper highest occupied molecular orbital (5.8 eV) than its aza[6]H counterpart (Supplementary Figs. 1–8), to reduce hole trapping in polymer blends (Fig. 1a). When blended with

F8BT at the same concentration (10 wt%) and processing conditions (160 nm thickness), both aza[6]H and monoF[6]H induce a chiral phase in the polymeric film. Annealed blends of (*P*)-aza[6]H give a dissymmetry factor of lower energy ( $\lambda = 491$  nm) transition of  $g_{\text{abs}} = 0.65$  (CD of 18,200 mdeg), whereas blends of (*P*)-monoF[6]H have a slightly lower but still substantial dissymmetry factor of  $g_{\text{abs}} = 0.42$  (CD of 12,000 mdeg; Fig. 1b and Supplementary Fig. 11). The CD of these films contains negligible contributions from linear dichroism and linear birefringence, with no CD sign inversion on rotation or flipping of the samples (Supplementary Figs. 13 and 14). This was further confirmed by Mueller matrix polarimetry (MMP) data showing that the CD elements  $m_{30}$  and  $m_{03}$  are symmetric whereas circular birefringence elements  $m_{21}$  and  $m_{12}$  are antisymmetric (Supplementary Figs. 15 and 16), which is consistent with prior studies on aza[6]H (ref. 8). This excludes any structural contributions to CPL, with the high chiroptical activity being attributed to the strong excitonic coupling between polymer-chain chromophores<sup>21</sup>. When optically excited, no change in the emitted CPL handedness is observed for a given enantiomer, regardless of the excitation geometry (Supplementary Figs. 18 and 19).

Conventional and inverted devices were fabricated with the same emissive layer thickness (160 nm). Conventional CP-OLEDs (Fig. 1c) of F8BT:(*P*)-aza[6]H blends with poly(9,9-dioctylfluorene-*alt*-*N*-(4-*sec*-butylphenyl)-diphenylamine) (TFB) as an additional hole transport layer (HTL) had lower efficiencies and higher turn-on voltages compared with F8BT:(*P*)-monoF[6]H-based devices (Supplementary Figs. 20 and 21). Furthermore, although the HTL is required to realize working CP-OLEDs for F8BT:(*P*)-aza[6]H blends, devices using F8BT:(*P*)-monoF[6]H can be fabricated HTL-free and maintain lower turn-on voltages compared with CP-OLEDs with aza[6]H (Supplementary Table 2). Inverted CP-OLEDs for all conditions (Fig. 1d) show higher device efficiencies compared with the conventional architecture (Supplementary Figs. 22 and 23). Consistent with conventional devices, inverted devices using F8BT:(*P*)-aza[6]H require tris(4-carbazoyl-9-ylphenyl)amine (TCTA) as an HTL, whereas F8BT:(*P*)-monoF[6]H-based CP-OLEDs can operate without an HTL. Inverted monoF[6]H-based CP-OLEDs demonstrate high efficiencies and, for HTL-free devices, very low efficiency roll-off (Supplementary Fig. 23 and Supplementary Table 2). The superior performance of CP-OLEDs incorporating F8BT:(*P*)-monoF[6]H confirms that the new chiral additive reduces the trapping caused by aza[6]H.

The lower density of trap states in F8BT:monoF[6]H blends is also supported by hole transport measurements via the space-charge-limited current method (Supplementary Figs. 24 and 25 and Supplementary Table 3). Almost three orders of magnitude difference in the hole mobility was observed in comparing blends of monoF[6]H and aza[6]H, with higher hole trap densities in aza[6]H blends. Mobility measurements of bilayers including an HTL reveal that for aza[6]H blends, the HTL improves hole mobility, whereas for monoF[6]H, it limits the injection of holes, pinning the RZ close to the anode in both cases. No differences in electron transport properties of the two additives were observed, even when measured in bilayers with an electron transport layer (Supplementary Fig. 25b and Supplementary Table 3). These measurements, performed using the same device stack as the respective CP-OLEDs, reveal that (1) in devices (conventional and inverted) with an HTL, the RZ is pinned near the HTL interface and (2) in HTL-free devices, the RZ is located closer to the centre of the stack due to balanced charge carrier injection and transport. This is consistent with the measured efficiency roll-off: efficiency roll-off is minimized in HTL-free devices due to the more balanced charge recombination and reduced quenching (Supplementary Fig. 27). Stability measurements further support this analysis, with conventional and inverted HTL-free devices showing improved stability compared with counterparts with an HTL (Supplementary Fig. 28). Capacitance–voltage (CV) and capacitance–frequency (CF) measurements indicate that devices with HTLs

suffer from charge accumulation and capacitance build-up due to the unbalanced charge carrier mobility and the pinned RZ close to the HTL. Specifically, HTL-free devices feature a sharp drop in capacitance after turning on in CV measurements, whereas devices with an HTL feature a capacitance build-up (Supplementary Fig. 29). CF measurements, carried out after device turn on, also feature a higher capacitance at low frequencies in HTL-free devices (Supplementary Fig. 30). Both these characterizations demonstrate charge accumulation and capacitance build-up due to unbalanced charge carrier mobility and support the location of the RZ near the interface with the HTL.

Enabled by the discovery of a chiral polymeric material with improved hole mobility, it was found that the handedness of CP-EL could be controlled through the use of conventional and inverted F8BT:(*P*)-monoF[6]H CP-OLEDs, with or without HTLs (Fig. 2). Without an HTL (Fig. 2a,b), the RZ of OLEDs using F8BT:(*P*)-monoF[6]H is in the middle of the active layer. The measured CP-EL retains the same handedness irrespective of the device architecture (preferentially left handed for the *P* enantiomer of monoF[6]H,  $g_{\text{EL,CONV}} = +0.10$  and  $g_{\text{EL,INV}} = +0.13$ ). This is the same handedness as optically pumped CP photoluminescence ( $g_{\text{PL}} = +0.24$ ). Together with the fact that the handedness of CPL cannot be inverted by changing the current flow direction, this suggests NCPE for F8BT:(*P*)-monoF[6]H CP-OLEDs without an HTL (Supplementary Figs. 33 and 35). Consistent with this assignment, measurements on semitransparent devices show the same magnitude and handedness of CP-EL regardless of the measurement direction:  $g_{\text{EL,ITO}} = +0.12$  and  $g_{\text{EL,AI}} = +0.10$  in the case of conventional semitransparent devices (Supplementary Fig. 33) and  $g_{\text{EL,ITO}} = +0.12$  and  $g_{\text{EL,AU}} = +0.10$  for inverted semitransparent devices (Supplementary Fig. 35). This is also consistent with the handedness of CPL emitted from thin films on optical excitation at different geometries. NCPE restricts the total  $g_{\text{EL}}$  of the device: the back electrode changes the phase of polarization, reversing its handedness and partially cancelling CPL emitted towards the transparent electrode ( $g_{\text{EL}} < g_{\text{PL}}$ ). The small differences in  $g_{\text{EL}}$  between conventional and inverted devices can be attributed to optical losses due to the attenuation of CPL propagating inside the device (Supplementary Note 3). For the same reason, the sum of  $g_{\text{EL}}$  obtained from semitransparent devices does not match the  $g_{\text{EL}}$  measured in devices with highly reflective electrodes.

In conventional devices with an HTL, the handedness of CP-EL inverts compared with devices without the HTL (Fig. 2c) and right-handed emission is preferred for the *P* enantiomer of monoF[6]H ( $g_{\text{EL,CONV}} = -0.40$ ). By contrast, left-handed emission is still preferred for the *P* enantiomer of monoF[6]H when used in inverted devices with an HTL ( $g_{\text{EL,INV}} = +0.38$ ; Fig. 2d). As such, the handedness of CPL is clearly inverted by changing the current flow direction for F8BT:(*P*)-monoF[6]H CP-OLEDs with an HTL, suggesting ACPE. Measurements using semitransparent devices showed that conventional devices with a TFB HTL gave opposite-handed CP-EL as a function of emission direction ( $g_{\text{EL,ITO}} = -0.22$  and  $g_{\text{EL,AI}} = +0.23$ ; Supplementary Fig. 34). Inverting the device structure when using TCTA as an HTL also results in opposite-handed CP-EL, but with the absolute handedness inverted relative to conventional devices with an HTL ( $g_{\text{EL,ITO}} = 0.33$  and  $g_{\text{EL,AU}} = -0.27$ ; Supplementary Fig. 36). The emission of CPL is non-reciprocal: CPL emitted towards the top electrode inverts handedness, partially combining with CPL emitted towards the ITO and increasing the measured  $g_{\text{EL}}$ . This overcomes the theoretical limit of devices with only NCPE ( $g_{\text{EL}} > g_{\text{PL}}$ ). Supplementary Fig. 37 evaluates the impact of HTL thickness in inverted devices, where the HTL is evaporated rather than solution processed. It is clear that the HTL thickness does not impact  $|g_{\text{EL}}|$ , but it does impact the EL lineshape due to cavity effects<sup>22</sup>.

In summary, the electrical control of CP-EL handedness is observed simply through the addition or omission of an HTL within the device stack. Devices without an HTL show NCPE, whereas devices with an HTL show APCE. In all the devices (that is, with ACPE and NCPE),  $g_{\text{EL}}$  is independent of current density, which is consistent with previous results in

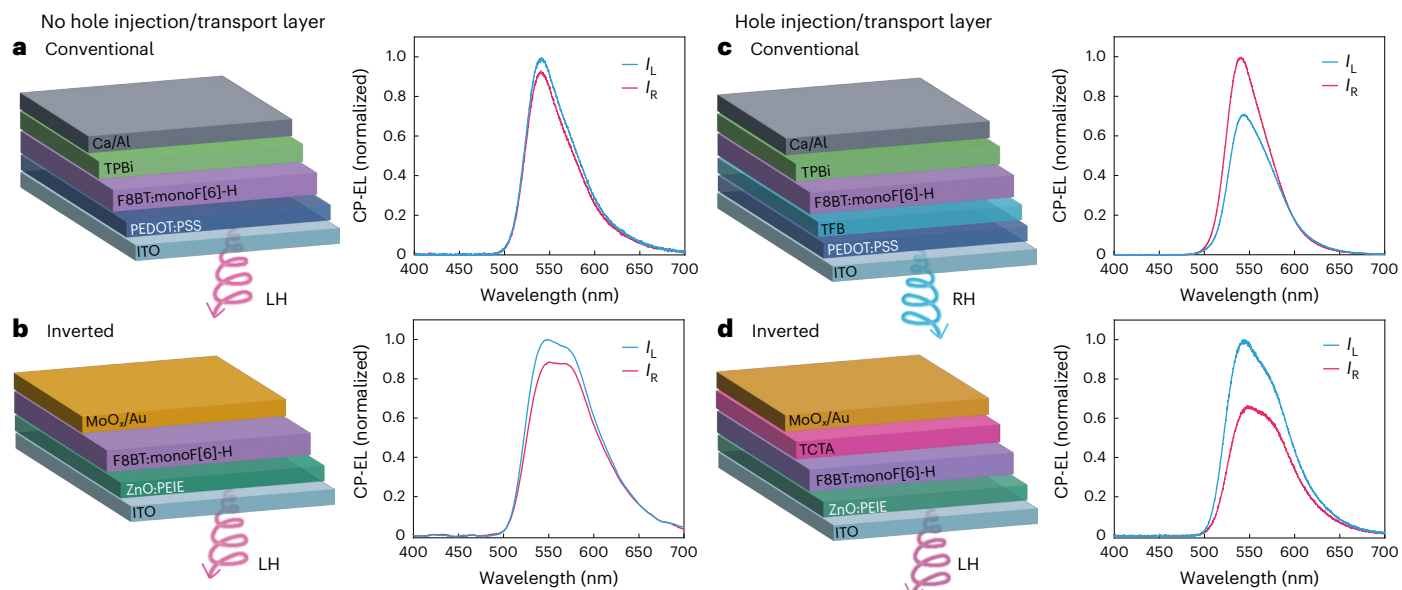


**Fig. 2 | Electrical control of CP-EL.** **a**, Device architecture (ITO/PEDOT:PSS/F8BT:monoF[6]H/TPBi/Ca/Al) and CP-EL characteristic of conventional HTL-free CP-OLEDs. **b**, Device architecture (ITO/ZnO/PEIE/F8BT:monoF[6]H/MoO<sub>3</sub>/Au) and CP-EL characteristic of HTL-free inverted CP-OLEDs. **c**, Device architecture (ITO/PEDOT:PSS/TFB/F8BT:monoF[6]H/TPBi/Ca/Al) and CP-EL characteristics of

conventional devices, with TFB as the HTL. **d**, Device architecture (ITO/ZnO/PEIE/F8BT:monoF[6]H/TCTA/MoO<sub>3</sub>/Au) and CP-EL characteristics of conventional devices, with TCTA as the HTL. The thickness of all emissive layers is 160 nm.  $I_L$ , intensity of left-handed (LH) light;  $I_R$ , intensity of right-handed (RH) light.

chiral polymer blends (Supplementary Fig. 38). Although the absolute  $g_{\text{EL}}$  values achieved in this work are not the highest reported so far, they remain among the highest in the field. This impressive performance is accompanied by the first demonstration of electrical control over the emission mechanism (Supplementary Table 5), achieved through careful material and device design.

## Discussion

We suggest that the measured CP-EL from CP-OLEDs using our chiral blend materials can be described with contributions from both ACPE and NCPE<sup>18</sup>:

$$I_L - I_R = \text{ACPE} + \text{NCPE}.$$

According to our previous theory and quantitative analysis of ACPE<sup>18</sup>, directional charge transport through chiral emissive layers induces OAM in CP-OLEDs<sup>23,24</sup>. We ignore the SAM of charge carriers because of negligible spin-orbital coupling in these organic polymers. There is a finite OAM transfer ( $\Delta l = l_e - l_h$ ) from charge carriers to photons during the electron-hole recombination process (Supplementary Note 2) and a given photon with finite  $\Delta l$  exhibits opposite handedness if it is emitted in opposite directions. Reversing the current directionality changes the sign of  $l_e$  ( $l_h$ ) due to the orbital-momentum locking in chiral materials<sup>18,23</sup>, and therefore, conventional and inverted devices emit CP-EL with opposite handedness. Through this mechanism, ACPE rationalizes the device-architecture-dependent CP-EL handedness in our devices that contain an HTL. When an HTL is used in conventional (HTL = TFB) or inverted (HTL = TCTA) devices, charge transport in the emissive layer is unbalanced towards electrons, pinning the RZ of the device to the HTL interface near the anode. Electrons injected from the cathode travel towards the HTL through the chiral active layer, recombining with holes at the interface. As such, in the presence of an HTL, electrons travel through the chiral active layer and gain OAM  $l_e$ , whereas holes travel through the achiral HTL and develop zero OAM ( $l_h = 0$ ). The finite OAM ( $\Delta l = l_e$ ) developed through the electron flow leads to ACPE, which overrides any NCPE in the system.

In devices without an HTL, charge injection and the transport of electrons and holes are balanced, and the RZ is in the centre of the active layer (Fig. 3a). Inversion of CP-EL handedness is not observed when switching the current direction or as a function of emission direction. The handedness of emitted light is the same as optically pumped CPL emission. In this balanced scenario, electrons and holes carry similar finite OAM ( $l_e \approx l_h$ ); therefore,  $\Delta l \approx 0$ , which suppresses ACPE. As such, only NCPE is observed. Thus, through adjusting the position of the RZ within a CP-OLED device using these materials, it is possible to tune the contribution of ACPE versus NCPE and, in turn, control the handedness of CP-EL for a fixed enantiomer of the emissive material.

The control of ACPE and NCPE in OLEDs requires a careful design of materials and devices. Materials capable of ACPE demonstrate a helical electron distribution such that the movement of charge carriers induces an OAM that is transferred to SAM in the emitted light. In the achiral luminescent polymer-chiral additive blend system considered here, twisted polymer backbones generate the appropriate topological electronic landscape. The additive should be designed such that it can induce a chiral phase and maintain the charge carrier properties of the achiral luminescent polymer. ACPE requires unbalanced, ambipolar charge transport in the emissive layer, which confines the RZ to a narrow region and pins the RZ position close to one of the electrodes. The RZ position is best controlled when the energy levels of the transport layer match those of the emissive layer, and requires selecting transport layers with a tuneable charge mobility.

## Summary

We have demonstrated that CP-EL handedness from a chiral polymer LED can be controlled electrically by tuning the charge carrier mobility and the RZ position, without changing the handedness or composition of the active layer. CPL emission in CP-OLEDs does not simply originate from the same mechanism of optically excited transitions (NCPE). The origin of this effect appears to be adjusting the interplay of NCPE versus ACPE through adjusting the balance of induced OAM in electrons versus holes. On a practical level, this strategy provides a simple means to access CP-OLEDs with high levels of

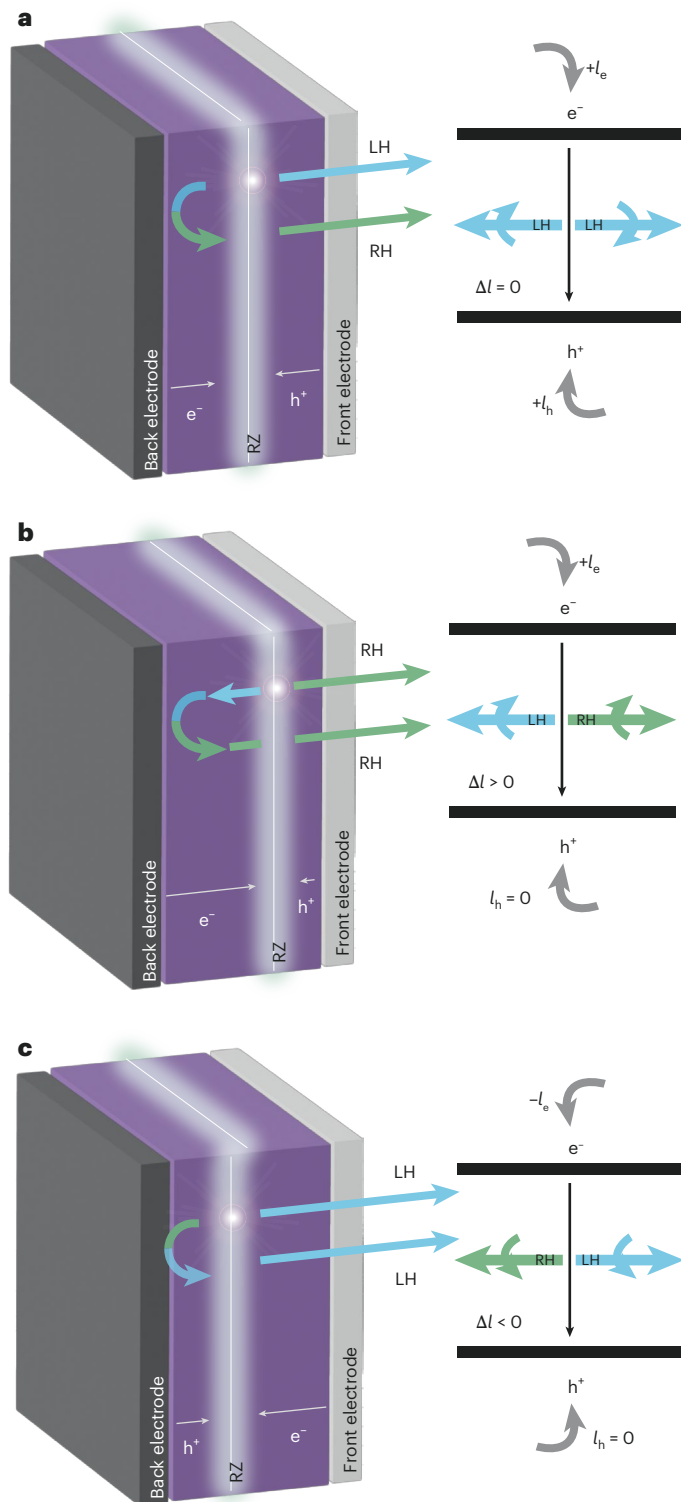


**Fig. 3 | Mechanisms inducing NCPE or ACPE.** **a**, NCPE occurs when there is balanced charge transport in the device through the omission of an HTL. **b,c**, ACPE occurs when charge transport is unbalanced towards electron transport through the addition of an HTL. For conventional devices, the RZ is close to the front electrode (**b**), whereas for inverted devices, the RZ is close to the back electrode (**c**). The positioning of the RZ controls the handedness of the ACPE through oppositely induced OAM.

CP-EL, where left- or right-handed CP-EL is available from a single emissive enantiomer.

Notable advances in the asymmetric synthesis of helicenes<sup>25</sup> means that it is increasingly simple to synthesize a single-enantiomer

chiral additive. If a single-enantiomer additive can be used to generate CP-OLEDs of either CP-EL handedness, this new CP-OLED strategy avoids the need for laborious and poorly scalable separation of racemic chiral additives into their separate enantiomers for CP-OLED usage. Thus, this approach provides a paradigm shift in the realization of organic CP-LEDs with controllable SAM information, which should enable many of the promised applications, from display technologies to quantum information systems. On a fundamental level, this study provides further evidence of the rich physics at play in chiral optoelectronic systems and suggests a means to control induced OAM in charge carriers within chiral semiconducting materials. Combining ACPE with other strategies, such as multilayer OLEDs or chiral microcavities<sup>26</sup>, could also enable new ways to boost the dissymmetric response of CP-LEDs. There continues to be high interest in the interplay of chirality, charge and spin, including through the expanding studies concerning chiral-induced spin selectivity<sup>20</sup>, and this study provides further materials and device frameworks for the characterization of these phenomena.

### Online content

Any methods, additional references, Nature Portfolio reporting summaries, source data, extended data, supplementary information, acknowledgements, peer review information; details of author contributions and competing interests; and statements of data and code availability are available at <https://doi.org/10.1038/s41566-025-01780-4>.

### References

1. Brandt, J. R., Salerno, F. & Fuchter, M. J. The added value of small-molecule chirality in technological applications. *Nat. Rev. Chem.* **1**, 0045 (2017).
2. Furlan, F. et al. Chiral materials and mechanisms for circularly polarized light-emitting diodes. *Nat. Photon.* **18**, 658–668 (2024).
3. Zhang, D. W., Li, M. & Chen, C. F. Recent advances in circularly polarized electroluminescence based on organic light-emitting diodes. *Chem. Soc. Rev.* **49**, 1331–1343 (2020).
4. Hirohata, A. & Takanashi, K. Future perspectives for spintronic devices. *J. Phys. D: Appl. Phys.* **47**, 193001 (2014).
5. Dainone, P. A. et al. Controlling the helicity of light by electrical magnetization switching. *Nature* **627**, 783–788 (2024).
6. Albano, G., Pescitelli, G. & Di Bari, L. Chiroptical properties in thin films of  $\pi$ -conjugated systems. *Chem. Rev.* **120**, 10145–10243 (2020).
7. Greenfield, J. L. et al. Pathways to increase the dissymmetry in the interaction of chiral light and chiral molecules. *Chem. Sci.* **12**, 8589–8602 (2021).
8. Wade, J. et al. Natural optical activity as the origin of the large chiroptical properties in  $\pi$ -conjugated polymer thin films. *Nat. Commun.* **11**, 6137 (2020).
9. Di Nuzzo, D. et al. High circular polarization of electroluminescence achieved via self-assembly of a light-emitting chiral conjugated polymer into multidomain cholesteric films. *ACS Nano* **11**, 12713–12722 (2017).
10. Jung, J. H., Lee, D. M., Kim, J. H. & Yu, C. J. Circularly polarized electroluminescence by controlling the emission zone in a twisted mesogenic conjugate polymer. *J. Mater. Chem. C* **6**, 726–730 (2018).
11. Lee, D. M., Kim, G. E., Kim, J. H. & Yu, C. J. Effects of molecular ordering on circularly polarized emission from a twisted mesogenic conjugated polymer. *J. Mater. Chem. C* **11**, 3300–3305 (2023).
12. Baek, K. et al. Simultaneous emission of orthogonal handedness in circular polarization from a single luminophore. *Light: Sci. Appl.* **8**, 93 (2019).
13. Albano, G., Pescitelli, G. & Di Bari, L. Reciprocal and non-reciprocal chiroptical features in thin films of organic dyes. *ChemNanoMat* **8**, e202200219 (2022).

14. Yang, Y., Da Costa, R. C., Smilgies, D. M., Campbell, A. J. & Fuchter, M. J. Induction of circularly polarized electroluminescence from an achiral light-emitting polymer via a chiral small-molecule dopant. *Adv. Mater.* **25**, 2624–2628 (2013).
15. Lee, D., Song, J., Lee, Y., Yu, C. & Kim, J. Control of circularly polarized electroluminescence in induced twist structure of conjugate polymer. *Adv. Mater.* **29**, 1700907 (2017).
16. Wan, L. et al. Inverting the handedness of circularly polarized luminescence from light-emitting polymers using film thickness. *ACS Nano* **13**, 8099–8105 (2019).
17. Wan, L., Wade, J., Wang, X., Campbell, A. J. & Fuchter, M. J. Engineering the sign of circularly polarized emission in achiral polymer—chiral small molecule blends as a function of blend ratio. *J. Mater. Chem. C* **10**, 5168–5172 (2022).
18. Wan, L., Liu, Y., Fuchter, M. J. & Yan, B. Anomalous circularly polarized light emission in organic light-emitting diodes caused by orbital-momentum locking. *Nat. Photon.* **17**, 193–199 (2023).
19. Zhang, Y. J., Oka, T., Suzuki, R., Ye, J. T. & Iwasa, Y. Electrically switchable chiral light-emitting transistor. *Science* **344**, 725–728 (2014).
20. Naaman, R., Paltiel, Y. & Waldeck, D. H. Chiral molecules and the electron spin. *Nat. Rev. Chem.* **3**, 250–260 (2019).
21. Laidlaw, B. et al. On the factors influencing the chiroptical response of conjugated polymer thin films. *Chem. Commun.* **57**, 9914–9917 (2021).
22. Wang, M., Lin, J., Hsiao, Y. C., Liu, X. & Hu, B. Investigating underlying mechanism in spectral narrowing phenomenon induced by microcavity in organic light emitting diodes. *Nat. Commun.* **10**, 1614 (2019).
23. Liu, Y., Xiao, J., Koo, J. & Yan, B. Chirality-driven topological electronic structure of DNA-like materials. *Nat. Mater.* **20**, 638–644 (2021).
24. Yan, B. Structural chirality and electronic chirality in quantum materials. *Annu. Rev. Mater. Res.* **54**, 97–115 (2024).
25. Gingras, M., Félix, G. & Peresutti, R. One hundred years of helicene chemistry. Part 2: stereoselective syntheses and chiral separations of carbohelicenes. *Chem. Soc. Rev.* **42**, 1007–1050 (2013).
26. Chen, T. L. et al. A 2D chiral microcavity based on apparent circular dichroism. *Nat. Commun.* **15**, 3072 (2024).

**Publisher's note** Springer Nature remains neutral with regard to jurisdictional claims in published maps and institutional affiliations.

**Open Access** This article is licensed under a Creative Commons Attribution 4.0 International License, which permits use, sharing, adaptation, distribution and reproduction in any medium or format, as long as you give appropriate credit to the original author(s) and the source, provide a link to the Creative Commons licence, and indicate if changes were made. The images or other third party material in this article are included in the article's Creative Commons licence, unless indicated otherwise in a credit line to the material. If material is not included in the article's Creative Commons licence and your intended use is not permitted by statutory regulation or exceeds the permitted use, you will need to obtain permission directly from the copyright holder. To view a copy of this licence, visit <http://creativecommons.org/licenses/by/4.0/>.

© The Author(s) 2025

<sup>1</sup>Department of Chemistry and Molecular Sciences Research Hub, Imperial College London, London, UK. <sup>2</sup>Centre for Processable Electronics, Imperial College London, London, UK. <sup>3</sup>Institute of Organic Chemistry and Biochemistry, Czech Academy of Sciences, Prague, Czech Republic. <sup>4</sup>Dipartimento di Chimica e Chimica Industriale, University of Pisa, Pisa, Italy. <sup>5</sup>Department of Materials, Imperial College London, London, UK. <sup>6</sup>Diamond Light Source, Harwell Science and Innovation Campus, Didcot, UK. <sup>7</sup>Department of Condensed Matter Physics, Weizmann Institute of Science, Rehovot, Israel. <sup>8</sup>Department of Physics, Pennsylvania State University, University Park, PA, USA. <sup>9</sup>Department of Chemistry, Chemistry Research Laboratory, University of Oxford, Oxford, UK. ✉e-mail: [matthew.fuchter@chem.ox.ac.uk](mailto:matthew.fuchter@chem.ox.ac.uk)

## Methods

### Materials

Aza[6]H was synthesized according to a previous report<sup>14</sup>, and monoF[6]H according to the synthesis procedure in the Supplementary Information and separated using preparative chiral high-performance liquid chromatography. F8BT and TFB were provided by Cambridge Display Technology. 2,2',2''-(1,3,5-Benzotriazolyl)-tris(1-phenyl-1*H*-benzimidazole) (TPBi) and TCTA were provided by Ossila.

### Thin film and device fabrication

All the substrates were cleaned via subsequent sonication for 10 min in deionized water, acetone and isopropanol, followed by 7 min of oxygen-plasma treatment. F8BT and (*P*)-aza[6]helicene (aza[6]H) or (*P*)-4-fluoro[6]helicene (monoF[6]H) were dissolved in toluene at 30 mg ml<sup>-1</sup> and blended to form a solution with 10% of chiral dopant. F8BT–chiral additive active layer blends were spin coated at different spin speeds (1,500–3,000 rpm) for 1 min to control the active-layer film thickness and annealed for 10 min in a nitrogen atmosphere (<0.1-ppm H<sub>2</sub>O and <0.1-ppm O<sub>2</sub>) at 140 °C. The film thickness was measured using a Dektak profilometer.

Hole-only devices for charge carrier mobilities were built on pre-patterned ITO glass (120 nm, 10 Ω). Poly(3,4-ethylenedioxythiophene) polystyrene sulfonate (PEDOT:PSS) was spin coated to achieve a 50-nm-thick film. If used, TFB was spin coated at 1,000 rpm for 1 min and annealed for crosslinking. The F8BT–chiral inducer active layer blend was then spin coated following the same procedure for thin films. If included, TCTA was evaporated with a thickness of 25 nm. Finally, 10 nm of MoO<sub>x</sub> and 80 nm of Au were thermally evaporated, defining a device area of 0.045 cm<sup>2</sup>.

Electron-only devices for charge carrier mobilities were built on Al-prepatterned glass. The F8BT–chiral inducer active layer blend was then spin coated at 2,000 rpm following the same procedure for thin films. Further, if included in the device, 10 nm of TPBi was thermally evaporated. Finally, 10 nm of Ca and 100 nm of Al were thermally evaporated, defining a device area of 0.045 cm<sup>2</sup>.

Conventional OLEDs were fabricated on prepatterned ITO glass (120 nm, 10 Ω). PEDOT:PSS was spin coated to achieve a 50-nm-thick film. If included in the device structure, TFB was spin coated at 1,000 rpm for 1 min and annealed at 180 °C for crosslinking. The active layer was then spin coated at 2,000 rpm following the same procedure for thin films. Finally, the device was completed with the thermal evaporation of 25 nm of TPBi, 10 nm of Ca and 100 nm of Al, defining an active device area of 0.045 cm<sup>2</sup>.

Inverted OLEDs were fabricated on prepatterned ITO glass (120 nm, 10 Ω). ZnO and ethoxylated polyethylenimine (PEIE) were spin coated following the already reported procedure. The active layer was then spin coated at 2,000 rpm following the same procedure for thin films. Finally, the device was completed with the thermal evaporation of TCTA, 10 nm of MoO<sub>x</sub> and 80 nm of Au, defining an active device area of 0.045 cm<sup>2</sup>.

### Photophysical characterization

CD measurements of thin films were carried out with a Chirascan (Applied Photophysics) spectrophotometer. CP photoluminescence was measured with a custom-built setup, using an achromatic quarter-wave plate (Thorlabs) and a linear polarizer with a 180° configuration (transmittance). Atomic force microscopy was measured using an Asylum MFP 3D device. Mueller matrix polarimetry in the transmission mode was carried out at the B23 beamline<sup>27</sup> at the Diamond Light Source.

### OLED characterization

Current–voltage–luminance (*J–V–L*) characterizations were carried out using a Keithley 2400 device and a Konica Minolta LS-160 luminance meter, with the emission profile assumed to be Lambertian. The

external quantum efficiency of the system was determined from the *J–V–L* characteristics and EL spectra, assuming Lambertian emission.

The CP-EL spectra were measured using a super-achromatic quarter-wave plate (Thorlabs SAQWP05M-700) and a visible wire grid linear polarizer (Thorlabs WP25M-VIS) placed in front of an Ocean Optics FL-4000 charge-coupled spectrophotometer, as previously reported<sup>28</sup>, and driving the device at a constant current (1 mA). The setup is automated via the integration of a rotation mount (Thorlabs ELL14K), ensuring the acquisition of left- and right-handed CP emission spectra in a time interval of <0.5 s to avoid potential  $g_{\text{EL}}$  artefacts due to device degradation. The quarter-wave plate is rotated with respect to the polarizer to avoid artefacts due to the relative orientation of the linear polarizer and the internal optical components of the charge-coupled spectrometer. This methodology ensures that the quarter-wave plate and polarizer are always correctly positioned, preventing unintentional birefringence or polarization artefacts that would otherwise need angle-dependent measurements and depolarization corrections. The dissymmetry factor ( $g_{\text{EL}}$ ) was calculated using the equation  $g_{\text{EL}} = 2(I_{\text{L}} - I_{\text{R}}) / (I_{\text{L}} + I_{\text{R}})$  at the maximum of the emission, with  $I_{\text{L}}$  and  $I_{\text{R}}$  being the left-handed and right-handed emission intensities, respectively.

### Data availability

Data supporting the findings of this study are available in the article and the Supplementary Information. Any additional information can be obtained from the corresponding authors upon reasonable request. Source data are provided with this paper.

### References

- Hussain, R., Jávorfí, T. & Siligardi, G. CD imaging at high spatial resolution at diamond B23 beamline: evolution and applications. *Front. Chem.* **9**, 616928 (2021).
- Moreno-Naranjo, J. M. et al. Enhancing circularly polarized electroluminescence through energy transfer within a chiral polymer host. *Adv. Mater.* **36**, 2402194 (2024).

### Acknowledgements

This work was supported by European Union's Horizon 2020 research and innovation programme under the Marie Skłodowska-Curie grant agreement number 859752 (M.J.F., J.W., N.G., I.G.S. and G.S.). This material was based on work supported by the Air Force Office of Scientific Research under award number FA9550-23-1-0633 (M.J.F. and J.W.). This work was supported by a grant from the Weizmann–UK Joint Research Program, award number 723018 (M.J.F. and B.Y.). MMP measurements were carried out at Diamond Light Source B23 beamline (SM32632 beamtime; J.W., M.J.F. and G.S.). This work has received funding from the Czech Science Foundation (registration number 24-10787S, I.G.S.) and IOCB CAS (RVO: 61388963, I.G.S.). B.Y. acknowledges the National Science Foundation through the Penn State Materials Research Science and Engineering Center (MRSEC) DMR 2011839. We would like to thank L. Bednářová for measuring the optical and chiroptical spectra of monoF[6]H.

### Author contributions

F.F. conceived the idea, proposed the project, designed the experiments, and fabricated and characterized the films and devices. D.N. contributed to the fabrication and measurements of semitransparent devices. M.Š., J.R. and I.G.S. designed and synthesized the new helicene additive. B.Y. contributed to the development and interpretation of the theoretical model. F.F., M.D.G., A.T. and G.S. carried out the thin-film measurements at beamline B32, with A.T. and G.S. contributing to the analysis of the Mueller matrix data. M.D.G. measured and analysed the atomic force microscopy data. F.F. wrote the initial paper with the help of J.W., N.G. and M.J.F. J.W., N.G. and M.J.F. provided guidance for the experiment design and data analysis.

M.J.F. supervised the project, assisted by J.W. and N.G. All authors contributed to the revision of the paper.

### Competing interests

The other authors declare no competing interests.

### Additional information

**Supplementary information** The online version contains supplementary material available at <https://doi.org/10.1038/s41566-025-01780-4>.

**Correspondence and requests for materials** should be addressed to Matthew J. Fuchter.

**Peer review information** *Nature Photonics* thanks Weibo Gao and Haipeng Lu for their contribution to the peer review of this work.

**Reprints and permissions information** is available at [www.nature.com/reprints](http://www.nature.com/reprints).